




## Detection of ferric ions in a gram-positive bacterial cell: *Staphylococcus aureus*

Erendra Manandhar, Ashley D. G. Johnson, William M. Watson, Shelby D. Dickerson, Gyan S. Sahukhal, Mohamed O. Elasri, Frank R. Fronczek, Peter J. Cragg & Karl J. Wallace

To cite this article: Erendra Manandhar, Ashley D. G. Johnson, William M. Watson, Shelby D. Dickerson, Gyan S. Sahukhal, Mohamed O. Elasri, Frank R. Fronczek, Peter J. Cragg & Karl J. Wallace (2021) Detection of ferric ions in a gram-positive bacterial cell: *Staphylococcus aureus*, Journal of Coordination Chemistry, 74:1-3, 380-401, DOI: [10.1080/00958972.2020.1868042](https://doi.org/10.1080/00958972.2020.1868042)

To link to this article: <https://doi.org/10.1080/00958972.2020.1868042>




View supplementary material 



Published online: 30 Dec 2020.



Submit your article to this journal 



Article views: 49



View related articles 



View Crossmark data 



## Detection of ferric ions in a gram-positive bacterial cell: *Staphylococcus aureus*

Erendra Manandhar<sup>a</sup>, Ashley D. G. Johnson<sup>a</sup>, William M. Watson<sup>a</sup>, Shelby D. Dickerson<sup>a</sup>, Gyan S. Sahukhal<sup>b</sup>, Mohamed O. Elasl<sup>b</sup>, Frank R. Fronczek<sup>c</sup>, Peter J. Cragg<sup>d</sup>  and Karl J. Wallace<sup>a</sup> 

<sup>a</sup>Department of Chemistry and Biochemistry, University of Southern Mississippi, Hattiesburg, MS, USA; <sup>b</sup>Department of Biological Sciences, University of Southern Mississippi, Hattiesburg, MS, USA; <sup>c</sup>Department of Chemistry, Louisiana State University, Baton Rouge, LA, USA; <sup>d</sup>School of Pharmacy and Biomolecular Sciences, University of Brighton, Brighton, UK

### ABSTRACT

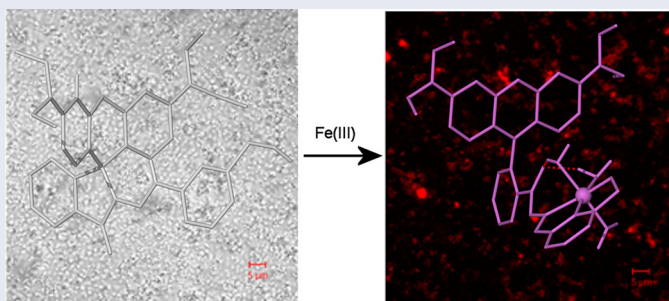
A rhodamine-based chemosensor was synthesized and found to selectively bind ferric ions over other metal ions ( $\text{Na}^+$ ,  $\text{K}^+$ ,  $\text{Ca}^{2+}$ ,  $\text{Mg}^{2+}$ ,  $\text{Fe}^{2+}$ ,  $\text{Zn}^{2+}$ ,  $\text{Cd}^{2+}$ ,  $\text{Co}^{2+}$ ,  $\text{Hg}^{2+}$ ,  $\text{Cr}^{3+}$ ,  $\text{Al}^{3+}$ ) in an organic-aqueous mixture ( $\text{CH}_3\text{CN-MES}$ ). Upon addition of ferric ions, the spirolactam ring opens, producing a visual color change and a fluorescence intensity increase, i.e. a “turn on” optical response at 577 nm is observed. The chemosensor coordinates to ferric ions in 1:1 stoichiometry with a calculated  $K_a = 3.5 \times 10^4 \text{ mol-dm}^{-3}$  by fluorescence spectroscopy and a LoD of 27 ppb. The chemosensor was reversible upon addition of the  $\text{Fe}^{3+}$  chelator desferrioxamine. One- and two-dimensional NMR experiments with  $\text{Al}^{3+}$  ions aided in understanding of the coordination environment of the ferric ion with the chemosensor, which were confirmed by molecular modelling calculations. X-ray quality crystals of the chemosensor were obtained, and the solid-state structure is reported. Confocal microscopy was used to detect free ferric ions in *Staphylococcus aureus*.

### ARTICLE HISTORY

Received 1 October 2020  
Accepted 7 December 2020

### KEYWORDS

Ferric ions; sensing; gram-positive bacteria; coordination; molecular probes



**CONTACT** Karl J. Wallace  [karl.wallace@usm.edu](mailto:karl.wallace@usm.edu)  Department of Chemistry and Biochemistry, University of Southern Mississippi, Hattiesburg, MS 39406, USA

Dedication: In honor of Jerry Atwood's 25 years' service to the Journal of Coordination Chemistry and his 51 years' service to the Chemistry World

 Supplemental data for this article is available online at <https://doi.org/10.1080/00958972.2020.1868042>.

© 2020 Informa UK Limited, trading as Taylor & Francis Group

## 1. Introduction

The synthesis of chemosensors to selectively detect biologically and environmentally essential ions is an area of extensive interest [1–3]. Iron is one of the most abundant metal ions in the human body, with 3–6 g present in the average adult living in the United States [4]. It is found predominantly in the +2 and +3 oxidation states and plays significant biological roles in the cell [5] where it is present at approximately 50–100  $\mu\text{M}$  (3 to 6 ppm) [3, 6]. The ferrous ion is utilized in oxygen metabolism, electron transfer, and DNA and RNA synthesis [7]. The ferric ion is less abundant but is nevertheless a critical metal ion, typically found in metallobiomolecules [8]. Also, a fraction of iron is “loosely” bound to organic anions (phosphates, citrates, carbonates, and carboxylates), polyfunctional ligands (polypeptides and siderophores), and surface components of membranes (phospholipid head groups) [9–11]. This can lead to labile iron pools (LIP’s) of free iron [7]. Moreover, iron can readily undergo redox reactions with molecular oxygen forming both  $\text{Fe}^{2+}$  and  $\text{Fe}^{3+}$  in these LIPs [10, 12]. The labile iron is a source for metabolic reactions that occur within the cell and is a site for generation of highly reactive oxygen species such as hydroxyl radicals *via* Fenton chemistry [13]. These highly reactive radicals can interact with many biologically important compounds such as sugars, lipids, proteins, and nucleic acids resulting in peroxidative tissue damage. It is also suggested the cellular toxicity caused by  $\text{Fe}^{3+}$  is potentially linked to conditions such as Alzheimer’s [14], Huntington’s [15], and Parkinson’s diseases [16, 17]. Conversely, deficiency of  $\text{Fe}^{3+}$  leads to anemia, kidney and liver damages, diabetes, and heart disease [18, 19]. Small-molecule recognition of iron in eukaryotic cells has been explored by Kumar [20, 21], Bhalla [22, 23], Kim [24, 25], Bernhardt [5, 26], Bruckner [27], Raymond, [28–30], Hider [31], and Critchon [29, 30], but, despite the role that iron plays in prokaryotic cells, i.e. bacterial cells, surprisingly few examples exist [32, 33]. The growth of many bacteria such as *Neisseria meningitidis* depends on the availability of iron [34]. Iron influences cell composition, metabolism, enzyme activity, and host cell interactions, including pathogenicity. The main functions of iron in the bacteria cell are catalytic [32, 35–37]. Iron often acts as a co-factor for different proteins whereby it can influence other components in the bacterial cell [38, 39]. For example, iron deficiency in *Mycobacterium smegmatis* decreases DNA and RNA levels [32]. Iron-promoted biofilm formation of *Pseudomonas aeruginosa* [40] is a significant problem for those with cystic fibrosis while the bacteria *Neisseria meningitidis* causes pyogenic meningitis and meningococcal septicemia in humans [34]. *Staphylococcus aureus* is responsible for both pneumonia and bacteremia and is the leading causes of skin and soft tissue infections such as abscesses, furuncles, and cellulitis [41].

Numerous small-molecule chemosensors can detect ferric ions in eukaryotic cells [42–44] but monitoring prokaryotic cells is less well explored, in particular Gram-positive bacteria. Furthermore, chemosensors specifically targeting ferric ions often lack selectivity. Many chemosensors also respond to competitive metal species such as  $\text{Al}^{3+}$ ,  $\text{Cu}^{2+}$ , and  $\text{Cr}^{3+}$  ions [45–47]. Literature reports often omit  $\text{Al}^{3+}$  ions from their studies, presumably due to the similarities in size and properties to the  $\text{Fe}^{3+}$  ion [42, 48]. Recently, our group has written a review article on chemodosimeters and chemo-reactants for sensing ferric ions, highlighting the area over the last several years [49], showcasing the need for chemosensors that selectively detect  $\text{Fe}^{3+}$  over  $\text{Al}^{3+}$ ,  $\text{Cu}^{2+}$  and  $\text{Cr}^{3+}$  ions.

## 2. Experimental

### 2.1. General techniques

One-dimensional ( $^1\text{H}$ ,  $^{13}\text{C}$ ) and two-dimensional (HMBC, HSQC, and ROESY) NMR spectra were recorded on a Bruker Ultrashield plus 400 MHz spectrometer in deuterated solvents or on a Bruker Advance 600 MHz spectrometer. Chemical shifts are reported in parts per million (ppm) downfield from tetramethylsilane (0 ppm) as the internal standard, and coupling constants ( $J$ ) are recorded in Hertz (Hz). The multiplicities in the  $^1\text{H}$  NMR spectra are reported as (br) broad, (s) singlet, (d) doublet, (dd) doublet of doublets, (ddd) doublet of doublet of doublets, (t) triplet, (sp) septet, and (m) multiplet. All spectra are recorded at ambient temperature. UV-Vis experiments were performed on a Beckman DU-70 UV-Vis spectrometer. Low-resolution mass spectra were measured with Finnigan TSQ70 and VG Analytical ZAB2-E instruments. IR spectra were recorded on a Nicolet Nexus 470 FT-IR paired with a Smart Orbit ATR attachment. Characteristic functional groups are reported in wavenumbers ( $\text{cm}^{-1}$ ). Fluorescence experiments were carried out on a QuantaMaster<sup>TM</sup> 400 intensity-based spectrofluorometer from PTI technologies in the steady-state; slit-widths 0.5 mm;  $\lambda_{\text{ex}} = 550 \text{ nm}$   $\lambda_{\text{em}} = 555 \text{ to } 800 \text{ nm}$ . Elemental analysis was carried out at Atlantic Microlab Inc.

### 2.2. General procedure UV-Vis and fluorescence experiments

Stock solutions of all compounds were prepared in  $\text{CH}_3\text{CN}$ , from which the desired concentration required for the optical studies were then made. A 20 or  $50 \mu\text{mol}\cdot\text{dm}^{-3}$  concentration solution was used for UV-Vis spectroscopy studies, and a  $5 \mu\text{mol}\cdot\text{dm}^{-3}$  solution concentration was used for the fluorescence studies. The absorption and emission data are shown in [Supporting information Figure S33](#). The solution was excited at  $\lambda = 550 \text{ nm}$  and scanned from 555 to 800 nm with slit widths set to 0.5 mm, for the fluorescence titration a  $500 \mu\text{mol}\cdot\text{dm}^{-3}$  of ferric perchlorate or triflate was prepared in  $\text{CH}_3\text{CN}$ . Aliquots of ferric perchlorate were added to **3**. Fluorescence spectra were recorded after each addition. Dilution factors were taken into consideration during binding studies. The binding constants were determined from fluorescence titrations using HypSpec 2006 [50].

### 2.3. Computational methods

Calculations were undertaken using the Spartan '18 Parallel Suite running on a Mac Pro with 3.5 GHz 6-Core Intel Xenon E5 processors and two threads per core.

### 2.4. X-ray crystallography

Data collection: COLLECT [51]; cell refinement: HKL SCALEPACK [52]; data reduction: HKL DENZO and SCALEPACK [52]; program(s) used to solve structure: SIR97 [53]; program(s) used to refine structure: SHELX2014/7 [54].

Crystal data for **3**,  $M = \text{C}_{35}\text{H}_{37}\text{N}_5\text{O}_3 \cdot 0.21\text{H}_2\text{O}$ ; F.W = 579.39, colorless needle fragment,  $0.34 \times 0.22 \times 0.20 \text{ mm}^3$ , monoclinic, space group  $P2_1/n$  (No. 14),  $a = 9.7604(4)$ ,  $b = 11.3709(6)$ ,  $c = 26.8708(11) \text{ \AA}$ ,  $\beta = 97.613(2)^\circ$ ,  $V = 2955.9(2) \text{ \AA}^3$ ,  $Z = 4$ ,  $D_c =$

$1.302 \text{ g}\cdot\text{cm}^{-3}$ ,  $F_{000} = 1232$ , Nonius KappaCCD,  $\text{MoK}\alpha$  radiation,  $\lambda = 0.71073 \text{ \AA}$ ,  $T = 90.0(5) \text{ K}$ ,  $2\theta_{\text{max}} = 55.7^\circ$ , 24901 reflections collected, 7029 unique ( $R_{\text{int}} = 0.0514$ ). Final  $\text{Goof} = 1.021$ ,  $R_1 = 0.0495$ ,  $wR_2 = 0.1015$ , with  $R$  indices based on 4498 reflections with  $I > 2(I)$  (refinement on  $F^2$ ), 406 parameters, 0 restraints.  $L_p$  and absorption corrections were applied,  $\mu = 0.085 \text{ mm}^{-1}$ .

## 2.5. $^1\text{H}$ NMR titrations

A solution of **3** ( $10.4 \text{ mmol}\cdot\text{dm}^{-3}$ ) was prepared by dissolving 3 mg in 0.5 mL  $\text{CD}_3\text{CN}$ . A 10-fold more concentrated solution of  $\text{Al}(\text{ClO}_4)_3$  was prepared in  $\text{CD}_3\text{CN}$ , and  $5 \mu\text{L}$  ( $5 \mu\text{L} = 0.1$  equivalents of metal salt) aliquots were added to the compound, and the  $^1\text{H}$  NMR spectrum recorded after each addition. Binding studies were undertaken by  $^1\text{H}$  NMR titrations using *HypNMR* 2016 [55]. The fully labeled numbering system (Supporting information Figure S5) and full 1D and 2D spectra of **3** and the  $\text{Al}^{3+}$  complex (Supporting information Figures S5–S27) are shown in the ESI.

## 2.6. Protocol for bacterial cell imaging

The stock solution of **3** in DMSO (10 mM) was prepared. The working solution was made by diluting the stock solution 10 times ( $200 \mu\text{L}$  **3** in  $1800 \mu\text{L}$  sterile 1X PBS or sterile distilled water). The final concentration of organic solvent utilized in cell growth was 10%.

Bacterial cells were grown in a tryptic soy agar plate from  $-80^\circ\text{C}$  freezer stock culture. A loopful of bacteria was inoculated into 5 mL of tryptic soy broth (TSB) and incubated overnight at  $37^\circ\text{C}$  with shaking at 200 rpm. The overnight bacterial cell culture was diluted 1:10 in 4 mL of pre-warmed TSB and further incubated at  $37^\circ\text{C}$  with shaking at 200 rpm for 3 h. After incubation,  $400 \mu\text{L}$  of  $\text{FeCl}_3$  (1 mM) was added to the culture yielding a final iron concentration of  $100 \mu\text{M}$ . Pre-warmed TSB ( $400 \mu\text{L}$ ) was added to the culture as a negative control. Both test and control cells were then incubated for 30 min. One mL of cells was aliquoted into 1.5 mL microfuge tube and centrifuged at  $10,000 \times g$  for 5 min to harvest the cells. Cells were washed twice with sterile distilled water. The supernatants were removed completely and discarded in each of the washing steps. The cells were resuspended in  $100 \mu\text{L}$  of  $1 \text{ mmol}\cdot\text{dm}^{-3}$  of **3** and  $20 \mu\text{L}$  of bacteria spotted on a clean glass slide, covered with the lifter slide, and the edges sealed. Confocal microscopy images were taken in 100 X/0.63 oil immersions. Phase-contrast photos were taken to visualize the cells, and the same field was laser scanned in cy3/rhodamine settings with emission at 550 nm and excitation at 580 nm. The same settings were used to scan both control and experimental (iron supplemented condition) for taking images, and the experiments were performed in triplicate to verify the result.

## 2.7. Synthesis of 2-amino-3',6'-bis(diethylamino)-2,3-dihydrospiro[isoindole-1, 9'-xanthene]-3-one (**1**) [56]

Rhodamine B (1.2 g, 2.5 mmol) was dissolved in ethanol (30 mL). Hydrazine hydrate (3.0 mL, 96 mmol) was then added dropwise with vigorous stirring at room temperature

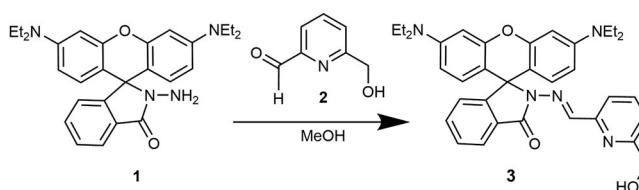
before being refluxed for 16 h. During this time, the solution turned from a dark purple to light orange. The solution was allowed to cool and the solvent was removed under reduced pressure. The oil was then dissolved in  $\text{CH}_2\text{Cl}_2$  (150 mL), washed with water (200 mL) and brine (200 mL), and dried over  $\text{Na}_2\text{SO}_4$ . The filtrate was evaporated to dryness, dissolved in  $\text{CH}_2\text{Cl}_2$  (30 mL), and stored at room temperature for 1–2 days. During this time, a white solid precipitated, the crystals were filtered and washed with  $\text{CH}_3\text{CN}$  (10 mL) to yield **2** (855 mg, 1.87 mmol, 75% yield).  $^1\text{H}$  NMR (400 MHz,  $\text{CDCl}_3$ , 300 K):  $\delta$  7.93–7.95 (m, 1H), 7.43–7.45 (m, 2H), 7.09 (m, 1H), 6.46 (d,  $J$  = 8.81 Hz, 2H), 6.42 (d,  $J$  = 2.49 8.80 Hz, 2H), 6.27–6.30 (dd,  $J$  = 8.84 and 2.52 Hz, 2H), 3.62 (br s, 2H), 3.34 (q,  $J$  = 6.78 Hz, 8H), 1.17 (t,  $J$  = 6.85 Hz, 12H) ppm.  $^{13}\text{C}$  NMR (100 MHz,  $\text{CDCl}_3$ , 300 K):  $\delta$  166.1, 153.9, 151.6, 148.9, 132.5, 130.0, 128.1, 128.0, 123.9, 123.0, 108.1, 104.6, 98.0, 65.9, 44.4, 12.7 ppm. IR (ATR solid); 3220–3350  $\nu_{\text{NH}_2}$  (vw), 2961  $\nu_{\text{C-H}}$  (w), 1761  $\nu_{\text{C=O}}$  (s)  $\text{cm}^{-1}$ .

## 2.8. Synthesis of 2-formyl-6-hydroxymethylpyridine (**2**) [57]

2,6-Bis(hydroxymethyl)pyridine (1.0 g, 7.2 mmol) was dissolved in hot  $\text{CHCl}_3$  (20 mL). The solution was cooled, and activated  $\text{MnO}_2$  (1.3 g, 14 mmol) was added slowly with stirring. The mixture was refluxed for 3 h. After this time, additional  $\text{MnO}_2$  (1.0 g, 11.6 mmol) was added and allowed to reflux for an additional 3 h. Then the reaction mixture was filtered hot through Celite. Upon cooling, the black inorganic salts were washed with  $\text{CH}_3\text{OH}$  ( $3 \times 25$  mL). The filtrate was concentrated under reduced pressure and the resulting oily residue was subjected to gradient column chromatography. Initially, the eluent started at ethyl acetate:hexane (1:9), with the pure product eluting with ethyl acetate:hexane (4:6) as a yellowish oil which turned into a solid after cooling (502 mg, 3.67 mmol g, 51%).  $^1\text{H}$  NMR (400 MHz,  $\text{CDCl}_3$ , 300 K):  $\delta$  10.09 (s, 1H), 7.87–7.89 (m, 2H), 7.53 (t,  $J$  = 4.39 Hz, 1H), 4.88 (s, 2H); IR (ATR solid); 3125  $\nu_{\text{O-H}}$  (br), 2715  $\nu_{\text{CHO}}$  (w), 1710  $\nu_{\text{C=O}}$  (s)  $\text{cm}^{-1}$ .

## 2.9. Synthesis of 2-(hydroxymethylpyridine)methyleneamine-spiro[isoindo-1,9'-xanthene]-3-one (**3**)

Compounds **1** (0.228 g, 0.5 mmol) and **2** (0.68 g, 0.5 mmol) were dissolved in  $\text{CH}_3\text{OH}$  (20 mL) and refluxed for 5–6 h. The solution was allowed to cool and stand at room temperature for 24 h, during which time crystals formed. These were filtered and washed with cold  $\text{CH}_3\text{OH}$  ( $3 \times 10$  mL) to yield the desired product as a light yellow solid; yield (215 mg, 0.37 mmol, 75%, m.p 245 °C).  $^1\text{H}$  NMR (400 MHz,  $\text{CD}_3\text{CN}$ , 300 K):  $\delta$  8.38 (s, 1H), 7.92 (d,  $J$  = 7.46 Hz, 1H), 7.70 (t,  $J$  = 7.71 Hz, 12H), 7.51–7.64 (m, 2H), 7.32 (d,  $J$  = 7.52 Hz, 1H), 7.05 (d,  $J$  = 7.39 Hz, 1H), 6.50 (d,  $J$  = 8.87 Hz, 1H), 6.45 (d,  $J$  = 2.51 Hz, 1H), 6.31–6.34 (dd,  $J$  = 8.87 and 2.55 Hz, 2H), 4.55 (d,  $J$  = 5.76 Hz, 1H), 3.48 (t,  $J$  = 5.78 Hz, 12H), 3.34 (q,  $J$  = 7.04 Hz, 8H), 1.10 (t,  $J$  = 7.01 Hz, 12H);  $^{13}\text{C}$  NMR (101 MHz,  $\text{CD}_3\text{CN}$ , 300 K):  $\delta$  164.5, 160.8, 152.7, 152.6, 152.1, 148.9, 145.5, 137.0, 133.8, 128.4, 127.9, 127.3, 123.1, 122.9, 120.4, 117.4, 117.4, 107.9, 105.0, 97.3, 65.1, 63.9, 43.6, 11.5 ppm. IR (ATR solid); 3435  $\nu_{\text{O-H}}$  (br), 2965, 2927, 2892  $\nu_{\text{C-H}}$  (w), 1703  $\nu_{\text{C=O}}$  (vs)  $\text{cm}^{-1}$ . LRMS-ESI;  $[\text{M} + \text{H}]^+ = 576.4$  (100%),  $[\text{M} + \text{Na}]^+ = 598.5$  (60%),  $[2\text{M} + \text{H}]^+ = 1150.8$  (20%),  $[2\text{M} + \text{Na}]^+ = 1173.1$  (37%). Anal. Calcd for  $\text{C}_{35}\text{H}_{37}\text{N}_5\text{O}_3$ : H 6.48%; N 12.18%; C 73.02%. Found for  $\text{C}_{35}\text{H}_{37}\text{N}_5\text{O}_3$ : H 6.45%; N 12.07%; C 72.55%.



**Scheme 1.** Synthesis of **3**.

### 3. Results and discussion

Rhodamine-based chemosensors have attracted attention since the work by Czarnik et al., who developed a molecular probe for  $\text{Cu}^{2+}$  ions in which the  $\text{Cu}^{2+}$  induced ring-opening of the lactam ring on the rhodamine B derivatives. This ring-opening produced a strong fluorescence signal upon hydrolysis of the chemodosimeter-copper $^{2+}$  adduct [58].

Xanthene derivatives have excellent photophysical properties; the neutral spirolactam ring is non-fluorescent and colorless but upon ring-opening produces a strong fluorescent signal ( $\lambda_{\text{em}} \approx 575 \text{ nm}$ ) and a distinct pink color ( $\lambda_{\text{ab}} \approx 560 \text{ nm}$ ) [59]. As a result of this ring opening and closing phenomenon, a number of rhodamine derivatives have been utilized to detect biologically relevant ions and biomolecules [59–61]. Consequently, the xanthene family of dyes is ideal molecular compounds from which to prepare an “off–on” chemosensor to detect ferric ions [62, 63].

Over the years, our group has designed and synthesized molecular probes for the monitoring of toxic analytes, including  $\text{Fe}^{3+}$  and  $\text{Zn}^{2+}$  [64–69], anions [70], and neutral species [71–73]. Our previously published systems, and those of many other groups, work well in organic solvents, which hinder their use in many biological or environmental applications. Preparing water-soluble chemosensors is an ongoing endeavor for our group. Here we describe the design and synthesis of a rhodamine B derived molecular probe that binds  $\text{Fe}^{3+}$  in *Staphylococcus aureus* and the chemosensor's ability to monitor ferric ions in a mixed organic-aqueous water system, using MES as a buffer at pH 5.5.

#### 3.1. Synthesis and pH studies

The commercially available rhodamine B was reacted with excess hydrazine hydrate to form 2-amino-3',6'-bis(diethylamino)-2,3-dihydrospiro[isoin-1,9'-xanthen]-3-one (**1**) in reasonable yield (75%). Compound **2** was prepared by reacting 2,6-bis(hydroxymethyl)pyridine with  $\text{MnO}_2$ , a commonly used mild oxidizing agent, often used to convert primary alcohols to aldehydes in the presence of other functional groups (ESI Supporting information Scheme S1) [74, 75]. Finally, **1** and **2** were coupled via a condensation reaction to form **3** as shown in Scheme 1.

It is well known that pH is crucial when using rhodamine-based molecular probes [44, 76]. Under acidic conditions, the spirolactam ring opens and pink color is observed along with a strong fluorescent signal observed at  $\lambda_{\text{em}} = 577 \text{ nm}$  in  $\text{CH}_3\text{CN}$ . The correct pH window must be chosen so that the initial optical state is in the lactam “off” form and, upon addition of metal ions, we can be confident that the fluorescence signal is due to coordination of ferric ions. This eliminates false positives from changes in pH that are encountered under physiological conditions. The optimum window for



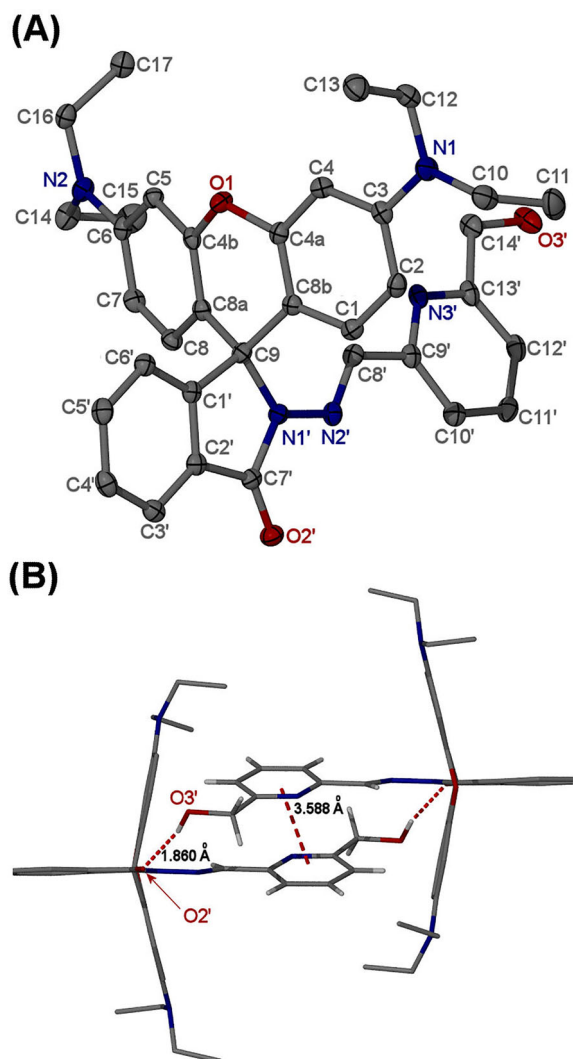


**Figure 1.** (A) The molecular structure of **3** showing displacement ellipsoids at the 50% probability level; a single H<sub>2</sub>O molecule has been omitted for clarity. (B) Crystal packing showing how two molecules are related in the unit cell.

chemosensor **3** in CH<sub>3</sub>CN is between pH 4 and 10 in the absence of metal ions (see ESI, [Supporting information Figure S1](#)), suggesting that the molecular probe is in the spiro-lactam form in this range.

### 3.2. X-ray crystallography and modeling calculations

Crystals of **3** were grown from a saturated methanolic solution over several days and crystallized in the monoclinic P2<sub>1</sub>/n space group ([Figure 1\(A\)](#)). There are two independent molecules in the asymmetric unit cell forming a dimer which is stabilized by C-H... $\pi$  (3.588 Å) and a single hydrogen bonding interaction between the hydroxyl group to the carbonyl oxygen (O3'-H3O'...O2' (D...A = 2.7345(17)) *via* an inversion center, generating the



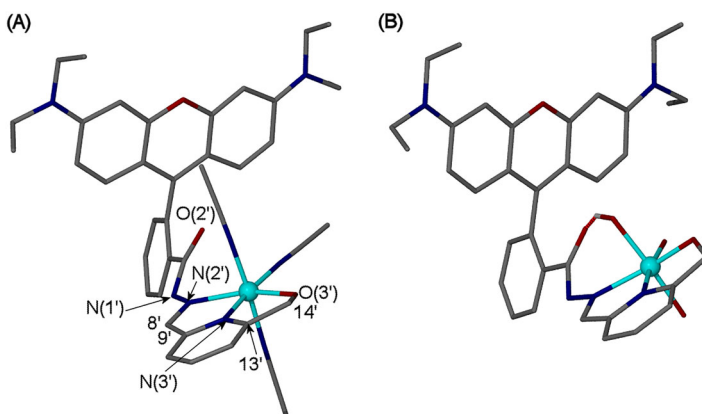


**Figure 2.** DFT fully optimized structures of (A)  $[\text{Fe}(\mathbf{3})(\text{CH}_3\text{CN})_3]^{3+}$  and (B)  $[\text{Fe}(\mathbf{3})(\text{H}_2\text{O})_3]^{3+}$  with hydrogens omitted for clarity.

two other molecules ( $z=4$ ) (see ESI, [Supporting information Figure S2](#)). The structure shows that the substituted phenyl ring, to which the metal ion is expected to ligate, is orthogonal to the xanthene ring ([Figure 1\(A\)](#)). This geometrical arrangement is typical for rhodamine molecules [77, 78]. However, a particularly interesting structural feature is the significant curvature of the xanthene ring systems ([Figure 1\(B\)](#)) as xanthenes are typically planar [79–82]. Numerous attempts were made to grow crystals from **3** and metal salts to no avail. To gain insight into possible ligand and coordination environments, a computational approach was adopted. An initial molecular geometry was generated using molecular mechanics energy minimization methods (Merck Molecular Force Field). The resulting atomic coordinates were used as the input to a semi-empirical calculation, where formal bonds were introduced between the solvent molecules and the metal center. Following geometry optimization, formal bonds were removed, and further refinement was undertaken by density functional methods (B3LYP/6-31G<sup>\*</sup>) to give a final geometry. Both the corresponding  $\text{Fe}^{3+}$  and  $\text{Al}^{3+}$  (see ESI, [Supporting information Figure S3](#)) coordination complexes were calculated. As solution studies were carried out in a mixture of  $\text{CH}_3\text{CN}$  ([Figure 2\(A\)](#)) and water ([Figure 2\(B\)](#)), both solvents were incorporated into the coordination sphere of the metal ion to mimic the solution work. The ferric ion is coordinated in a tridentate fashion, occupying the equatorial positions, forming two five-membered chelating ring systems. Solvent molecules occupy the remaining sites. The tris-aqua compound seems to be stabilized by a water molecule bound in the axial position, which participates in an intramolecular hydrogen bonding interaction with the carbonyl group. The same coordination environment is seen in the  $\text{Al}^{3+}$  complex (see ESI, [Supporting information Figure S3B](#)).

### 3.3. IR Spectroscopy

In order to verify the binding mode of  $\text{Fe}^{3+}$  suggested by the molecular modeling calculations, an IR study was conducted. The infrared spectrum of free chemosensor **3** was recorded as a solid using an ATR-FTIR and compared with that of the metal complex. A 1:1 ratio of **3** and  $\text{Fe}(\text{ClO}_4)_3$  was refluxed in  $\text{CH}_3\text{CN}$  overnight, evaporated to dryness, and the resulting solid allowed to air dry over several days. The pink/red solid

was used to take an IR spectrum of the complex. Chemosensor **3** has distinctive functional groups that are excellent IR handles to help our understanding of the coordination environment, as we were unable to grow crystals of the coordination complex. The carbonyl group on the phenyl moiety has a characteristic IR stretching band at  $1703\text{ cm}^{-1}$  and a hydroxyl group at  $3435\text{ cm}^{-1}$ , typical for hydrogen bonding interactions (see ESI, [Supporting information Figure S4A](#)), supporting the hydrogen bonding interaction seen in the crystal structure. The stretching band assigned to the carbonyl group at  $1703\text{ cm}^{-1}$  is shifted to lower wavenumber and seen at  $1645\text{ cm}^{-1}$  in the  $[\text{Fe}(\mathbf{3})]^{3+}$  complex. Upon coordination of the iron, the carbonyl group on the phenyl ring loses its double bond character as the functional group now participates in coordination with  $\text{Fe}^{3+}$ . The appearance of a sharp stretching band at  $619\text{ cm}^{-1}$  is indicative of a Fe-OH bond (see ESI, [Supporting information Figure S4B](#)) [83] that also participates in hydrogen bonding (see ESI, [Supporting information Figure S4C](#)). This is supported by change in the C=O stretching frequency. Moreover, the analogous stretch in the ionic iron perchlorate hydrate spectrum is weak and broad. Additionally, the appearance of several broad bands between  $3000$  and  $3500\text{ cm}^{-1}$  is also indicative of the presence of coordinated water molecules (see ESI, [Supporting information Figure S4A](#)).

Significant infrared spectral changes occur when perchlorate coordinates to a metal ion through different modes [84]. Determination of the binding mode due to changing symmetry of the  $\text{ClO}_4^-$  ion upon binding, from  $T_d$  (ionic) to  $C_{3v}$  (unidentate) and  $C_{2v}$  (bidentate or bridging), can help identify the binding mode of the anion [85–87]. The IR spectrum of ionic  $\text{Fe}(\text{ClO}_4)_3$  shows a broad symmetrical band at  $1043\text{ cm}^{-1}$ , typical of the  $T_d$  symmetry of the ion (see ESI, [Supporting information Figures S4C](#)). The anion in the complex shows distinctive degeneracies, presumably due to the counterion hydrogen bonding to the water molecules coordinated, which subsequently changes the  $T_d$  to  $C_{3v}$ . This is in agreement with our previously published work [66].

### 3.4. $^1\text{H}$ NMR studies

To obtain an understanding of the binding environment, we carried out 1D and 2D NMR experiments, although, due to the paramagnetic nature of  $\text{Fe}^{3+}$  ions, we were unable to perform NMR experiments directly with ferric salts. However, the  $\text{Al}^{3+}$  ion is diamagnetic, with an ionic radius of  $0.54\text{ \AA}$ , which is similar to  $\text{Fe}^{3+}$  ions ( $0.55\text{ \AA}$ ), additionally,  $\text{Al}^{3+}$  ions are known to have common coordination numbers of four and six, making  $\text{Al}^{3+}$  ion an excellent substitute for ferric ions in the structural elucidation studies. The 1D and 2D NMR spectra of chemosensor **3** and the  $[\text{Al}(\mathbf{3})]^{3+}$ , prepared *in situ* by adding one equivalent of  $\text{Al}(\text{ClO}_4)_3$  to **3**, are shown in the Supporting Information ([Supporting information Figures S5–S27](#)). Even though  $\text{Al}^{3+}$  ions do not display any optical response at the  $\mu\text{M}$  concentration (*vide infra*), it is expected that at significantly higher concentration (mM range) the equilibrium can be shifted towards  $[\text{Al}(\mathbf{3})]^{3+}$  product. This is advantageous as this concentration is now within the NMR concentration limits to aid in our understanding of the coordination environment.

The proton and carbon chemical environments close to the coordination environment had the greatest chemical shift change as shown in [Figure 3](#). The imine proton C(8')H has the most significant downfield chemical shift ( $\Delta 1.2\text{ ppm}$ ), consistent with

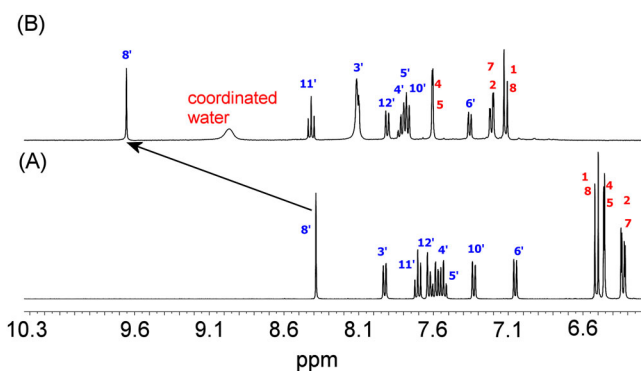


**Figure 3.** Partial  $^1\text{H}$  NMR of **3** (A) alone and upon addition of 1.2 equivalents of  $\text{Al}(\text{ClO}_4)_3$  in  $\text{CD}_3\text{CN}$ .

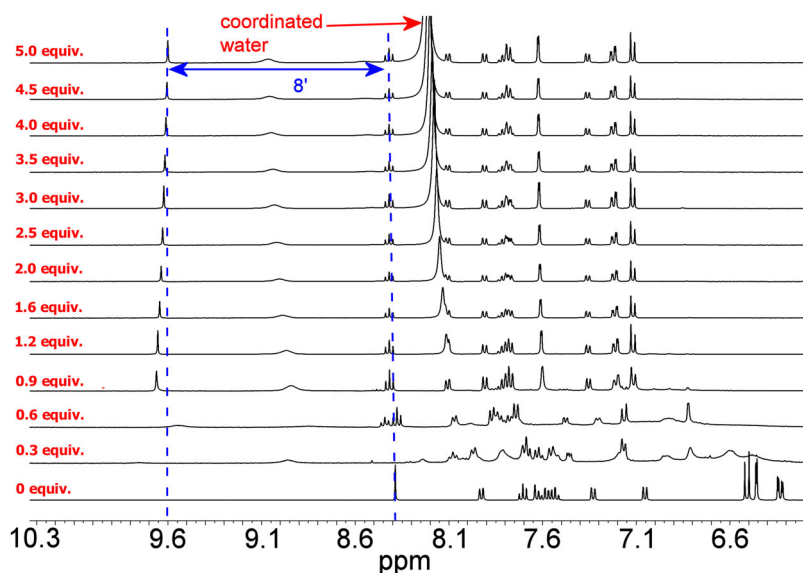


**Figure 4.**  $^1\text{H}$  NMR titration between **3** and  $\text{Al}(\text{ClO}_4)_3$  in  $\text{CD}_3\text{CN}$ ,  $\log K_{11} > 7$ .

the nitrogen coordinating to the metal center thereby making the proton more acidic, and a considerable upfield carbon shift ( $\Delta$  6.2 ppm) is observed. A distinct triplet is seen at 3.48 ppm, which can be assigned to the hydroxyl group, which disappears upon metal coordination, supporting the binding of the oxygen to  $\text{Al}^{3+}$ . As a number of the protons produced significant chemical shifts we carried out a  $^1\text{H}$  NMR titration of **3** by adding aliquots of  $\text{Al}(\text{ClO}_4)_3$  in  $\text{CD}_3\text{CN}$  (Supporting information Table S1). There were significant downfield chemical shifts in  $^1\text{H}$  NMR signals upon addition of  $\text{Al}^{3+}$  for the protons of imine C(8')H, the methylene group C(14')H, and protons on the pyridine ring. The changes in chemical shifts for C(8')H, C(14')H, and C(11')H after addition of one equivalent of  $\text{Al}(\text{ClO}_4)_3$  were 1.3, 0.4, and 0.7 ppm, respectively (Figure 4 and ESI, Supporting information Figures S28 and S29). Downfield shifts of pyridine protons can be explained by the inductive effect when the  $\text{Al}^{3+}$  ion is coordinated to the pyridine nitrogen. The protons on the xanthene moiety also shift significantly in the

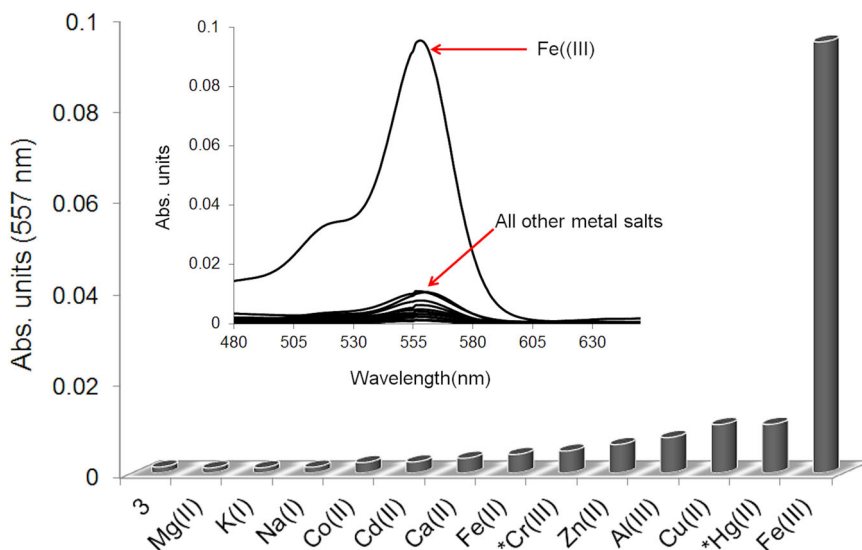


**Figure 5.** UV-Vis optical screening of metal salts with **3** ( $50 \mu\text{mol}\cdot\text{dm}^{-3}$  in  $\text{CH}_3\text{CN}$  upon addition of three equivalents of metal ions, as their  $\text{ClO}_4^-$  salts (\*Cl $^-$  salt).

downfield direction upon addition of  $\text{Al}^{3+}$  ions. This is due to the conjugation and decrease in electron density of the xanthene ring once spiro lactam ring of **3** opens because of binding to  $\text{Al}^{3+}$ . No further chemical shifts were observed after the addition of one equivalent of  $\text{Al}(\text{ClO}_4)_3$  (Figure 4). The binding affinity between **3** and  $\text{Al}^{3+}$  could not be calculated by nonlinear regression due to the high concentration used for the NMR experiments ( $0.01 \text{ mol}\cdot\text{dm}^{-3}$ ) and only an approximate  $K_{11}$  value could be obtained ( $\log K > 7$ ) using *HypNMR* (see ESI, Supporting information Figure S30) [55].

### 3.5. Optical studies

#### 3.5.1. UV-Vis spectroscopy

The spectroscopic response of **3** was initially investigated by screening a range of biologically relevant metal ions ( $\text{Na}^+$ ,  $\text{K}^+$ ,  $\text{Ca}^{2+}$ ,  $\text{Mg}^{2+}$ ,  $\text{Zn}^{2+}$ ,  $\text{Cd}^{2+}$ ,  $\text{Co}^{2+}$ ,  $\text{Fe}^{2+}$ ,  $\text{Cu}^{2+}$ ,  $\text{Hg}^{2+}$ ,  $\text{Cr}^{3+}$ ,  $\text{Al}^{3+}$ , and  $\text{Fe}^{3+}$ ) by adding  $150 \mu\text{mol}\cdot\text{dm}^{-3}$  of metal salts into a solution of  $\text{CH}_3\text{CN}$ . The initial UV-Vis spectrum of **3** does not show the typical absorption band at 557 nm for rhodamine compounds, therefore the molecule is in the "off" state. Upon addition of  $150 \mu\text{mol}\cdot\text{dm}^{-3}$  ferric ions to **3**, the solution turned from colorless to pink. The absorption band at 557 nm can be attributed to the ring opened form because of coordination of  $\text{Fe}^{3+}$ . No other metal ions ( $\text{Na}^+$ ,  $\text{K}^+$ ,  $\text{Ca}^{2+}$ ,  $\text{Mg}^{2+}$ ,  $\text{Cr}^{3+}$ ,  $\text{Al}^{3+}$ ,  $\text{Fe}^{2+}$ ,  $\text{Zn}^{2+}$ ,  $\text{Cd}^{2+}$ ,  $\text{Co}^{2+}$ ,  $\text{Hg}^{2+}$ ) gave a color change (Figure 5).

The UV-Vis screening studies suggest that **3** could serve as a "naked-eye" chemosensor towards ferric ions in  $\text{CH}_3\text{CN}$  and  $\text{CH}_3\text{CN}$  aqueous mixture (MES buffer at pH 5.5). A UV-Vis titration was carried out with  $\text{Fe}(\text{triflate})_3$ . The counter-ion also plays a role in the speciation; both the triflate and perchlorate salts were used and did not affect the calculated binding constants [88]. The binding affinity was calculated using the nonlinear regression program *HypSpec* [50, 89]. To obtain a good fit between the

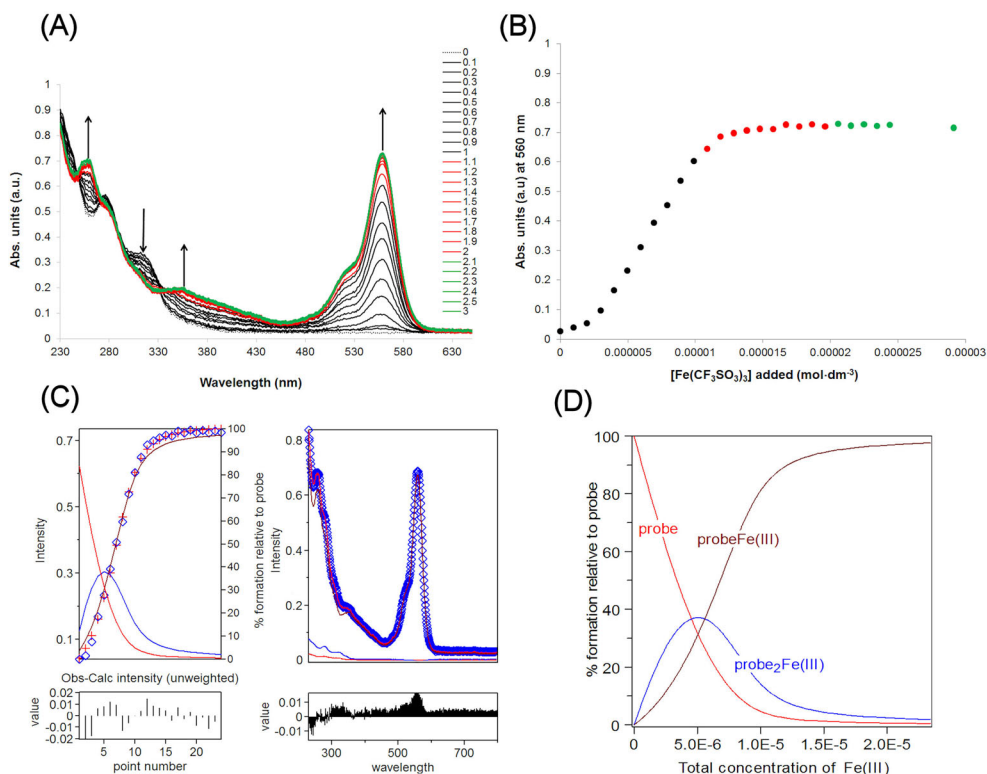


**Figure 6.** (A) UV-Vis titration between **3** upon addition of  $\text{Fe}(\text{CF}_3\text{SO}_3)_3$  in a  $10 \mu\text{mol}\cdot\text{dm}^{-3}$  in  $\text{CH}_3\text{CN}$ , (B) binding isotherm, (C) *HypSpec 2014* [50] data and (D) *HySS 2009* [89] simulated binding isotherms, in excellent agreement with the experimental data.

observed experimental data and the model, different speciations had to be included. An example of the UV-vis titration data is shown in Figure 6. Ferric triflate was added to probe **3** in  $\text{CH}_3\text{CN}$ . The UV-Vis spectra and the experimental binding isotherm are shown in Figure 6(A,B), respectively. As the rhodamine dye ring opens, a hyperchromic shift is seen at 560 nm. Moreover, a band at 375 nm suggests that the ferric ion has coordinated to the molecular probe. The 1:1 binding stoichiometry between **3** and  $\text{Fe}^{3+}$  ions was calculated to have an association constant of  $\log K_{11} = 6.9$ . Figure 6(C,D) show the least-squares fitting from the experimental data in Figure 6(B) and the simulated binding isotherms (Figure 6(D)), which is in excellent agreement with the fit.

Monitoring and probing ferric ions in an aqueous environment is incredibly challenging. The concentration of ferric ions is very low under physiological conditions,  $[\text{Fe}(\text{H}_2\text{O})_6]^{3+} 10^{-18} \text{ M}$ , [90], therefore organic ligands with a high affinity for ferric ions ( $K_{\text{aff}} > 10^{30}$ ) need to be used to bind iron in the +3 oxidation state (siderophores) [91–93]. Another factor affecting the concentrations of ferric and ferrous ions in water is the speciation of the metal, and this factor is often overlooked in the sensing community [94].

The hydrolysis of ferric ions in aqueous solutions is a convoluted time-dependent system. It can be defined as hydrolysis-polymerization-precipitation. A simple mechanism describes the process in several steps: (a) primary hydrolysis giving rise to low-

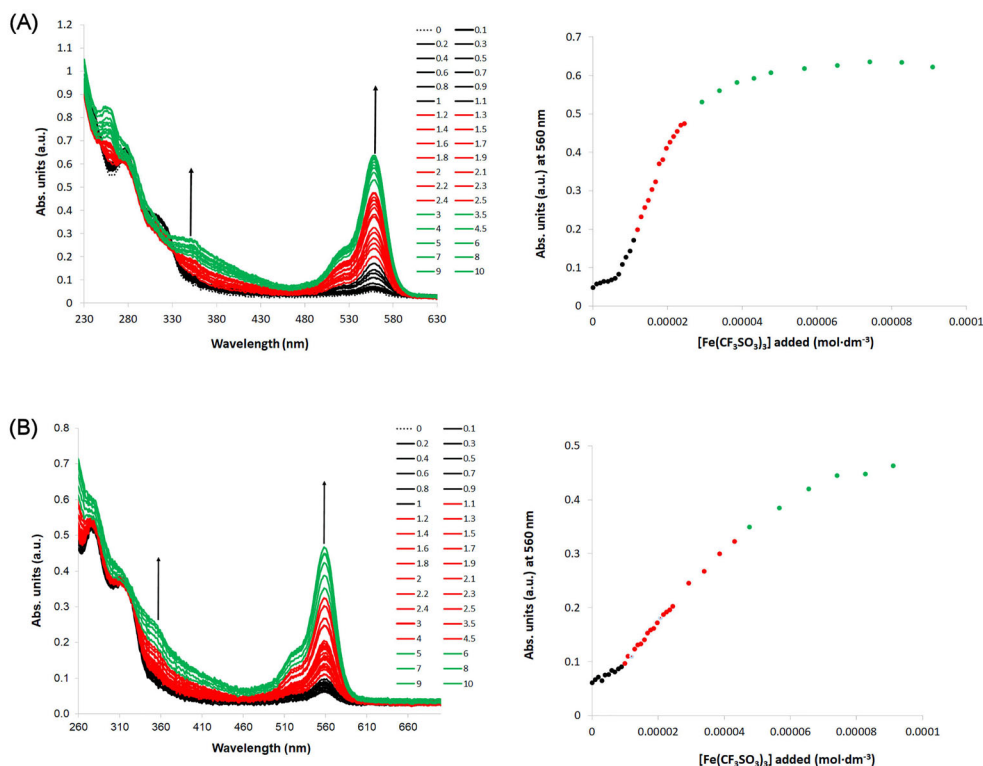


**Figure 7.** UV-Vis titration (spectra and binding isotherms) between **3** upon addition of  $\text{Fe}(\text{CF}_3\text{SO}_3)_3$  in a  $10\ \mu\text{mol}\cdot\text{dm}^{-3}$  solution in (A)  $\text{CH}_3\text{CN}:\text{MES}$  (95:5) and (B)  $\text{CH}_3\text{CN}:\text{MES}$  (90:10).

molecular-weight complexes (monomer and dimer), i.e.  $\text{Fe}(\text{OH})^{2+}$ ,  $\text{Fe}(\text{OH})_2^+$ ,  $\text{Fe}_2(\text{OH})_2^{4+}$ ; (b) formation and aging of polynuclear polymers, i.e.  $\text{Fe}_n(\text{OH})_m(\text{H}_2\text{O})_x^{(3n-m)+}$  or  $\text{Fe}_n\text{O}_m(\text{OH})_x^{(3n-2m-x)+}$ ; (c) precipitation of ferric oxides and hydroxides, i.e.  $\text{Fe}(\text{OH})_3$ ,  $\text{FeOOH}$ , and  $\text{Fe}_2\text{O}_3$ . The whole process, from hydrolysis to precipitation, can take several years [95–99], however, initial hydrolysis is very rapid [95]. Different concentrations of ferric species over a given pH range have been reported in predominance diagrams at  $25^\circ\text{C}$  [100]. Dimeric iron species have also been seen in solid-state structures. For example, the dimeric  $[\text{Fe}_2(\text{OH})_2]^{4+}$  ion has been suggested as the first condensation product of  $[\text{Fe}(\text{OH}_2)_6]^{3+}$ , but with little evidence (outside kinetics), reported as far back as Cotton and Wilkinson 1st edition [101]. In fact, hard evidence is in favor of a  $\mu$ -oxo bridged species, as first shown by Junk *et al.* isolating  $[(\text{H}_2\text{O})_5\text{Fe}-\text{O}-\text{Fe}(\text{H}_2\text{O})_5]^{4+}$  in the solid state as crown ether adducts characterized by X-ray diffraction [102]. *In situ* studies by EXAFS on ferric nitrate solutions identified the  $\mu$ -oxo bridged dimer in solutions [103].

Despite substantial research on iron hydrolysis reactions, a significant amount of conjecture remains with respect to the stability of iron hydrolytic species [104]. The predominance diagrams suggest that at deficient iron concentrations, it is possible to inhibit the formation of iron hydroxide precipitates in solution. One drawback of this, however, is that extremely sensitive analytical techniques would be required to measure the concentration of iron complexes in solution precisely. To investigate the effect of molecular probe **3** in an aqueous environment, we carried out UV-vis titrations

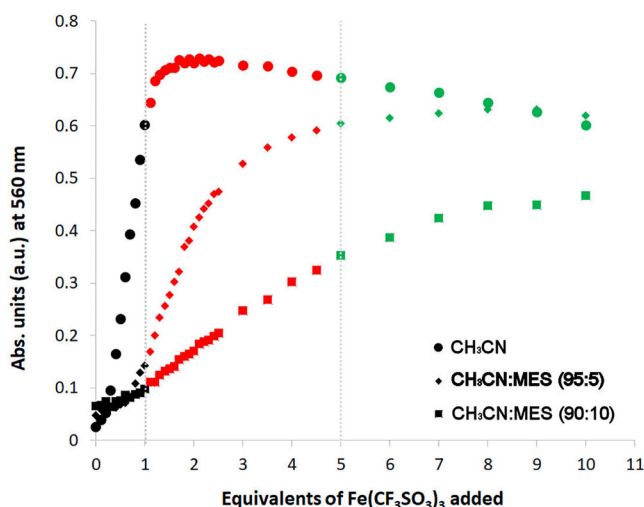


**Figure 8.** A comparison of the binding isotherms obtained between **3** and  $\text{Fe}(\text{CF}_3\text{SO}_3)_3$  in a  $10 \mu\text{mol}\cdot\text{dm}^{-3}$  solution in  $\text{CH}_3\text{CN}$ ,  $\text{CH}_3\text{CN}:\text{MES}$  (95:5) and  $\text{CH}_3\text{CN}:\text{MES}$  (90:10) (MES pH = 5.5, 10 mM).

**Table 1.** Binding constant ( $\beta$ ) determined by UV-Vis titrations for the interaction between **3** and ferric triflate, in different solvent systems.

Probe <b>3</b>	$^aK_{11} (\text{M}^{-1})$	$K_{12} (\text{M}^{-2})$	$K_{21} (\text{M}^{-2})$	$\beta$
$\text{CH}_3\text{CN}$	$7.76 \times 10^6$	$6.17 \times 10^4$	—	$4.79 \times 10^{11}$
$\text{CH}_3\text{CN}:\text{MES}$ (95:5)	$1.20 \times 10^7$	—	$1.51 \times 10^5$	$1.82 \times 10^{12}$
$\text{CH}_3\text{CN}:\text{MES}$ (90:10)	$2.07 \times 10^7$	—	$3.16 \times 10^3$	$6.54 \times 10^{10}$

<sup>a</sup> $K$  values were obtained from HypSpec 2016. Different binding species had to be taken into account when fitting the nonlinear regression data. Errors in  $K_{11}$  are <5%.  $K_{11} = [\text{Fe}(3)]^{3+}$ ;  $K_{12} = [\text{Fe}(3)_2]^{3+}$ ;  $K_{21} = [\text{Fe}_2(3)]^{3+}$ .

between **3** and ferric triflate in a  $\text{CH}_3\text{CN}$  and MES buffer (pH = 5.5; 10 mM) (Figure 7). Initially, the UV-Vis titration behaves similar to the 100%  $\text{CH}_3\text{CN}$  study. However, as the MES buffer concentration increases the shape of the binding isotherm changes, and the binding isotherm appears to continuously increase, without reaching saturation, until five equivalents. The UV-Vis spectra, shown in Figures 7(A,B), show absorbance intensity increases. This increase is indicative of other ferric species in solution, most likely ferric hydroxide solid particulate that rapidly forms in the organic-aqueous media in the experiment, which means that the ferric hydrolysis is occurring quicker than binding between **3** and ferric ions. This is reasonable, as the binding environment in **3** does not resemble that of a siderophore motif and merely binds tridentate.

As the water content is increased, the shape of the binding isotherm changes; in a noncompetitive solvent, like  $\text{CH}_3\text{CN}$ , a typical 1:1 binding isotherm is obtained. As the competitive nature of the medium increases from 5% to 10% (MES buffer pH = 5.5), the binding isotherms differ significantly (Figure 8).  $K_{11}$  is approximately the same ( $K_{11} \approx \log 7$ ), Table 1 (ESI, Supporting information Figures S34 and S35). However, the model used to calculate the binding constants required different species to be part of the non-linear fit algorithm. In the organic solvent, a 2:1 (2 x probe **3**: $\text{Fe}^{3+}$ ) was needed, but in both of the aqueous systems, the speciation was 1:2 (probe **3**: 2 x  $\text{Fe}^{3+}$ ). This agrees with our understanding of the aqueous chemistry of ferric ions. As



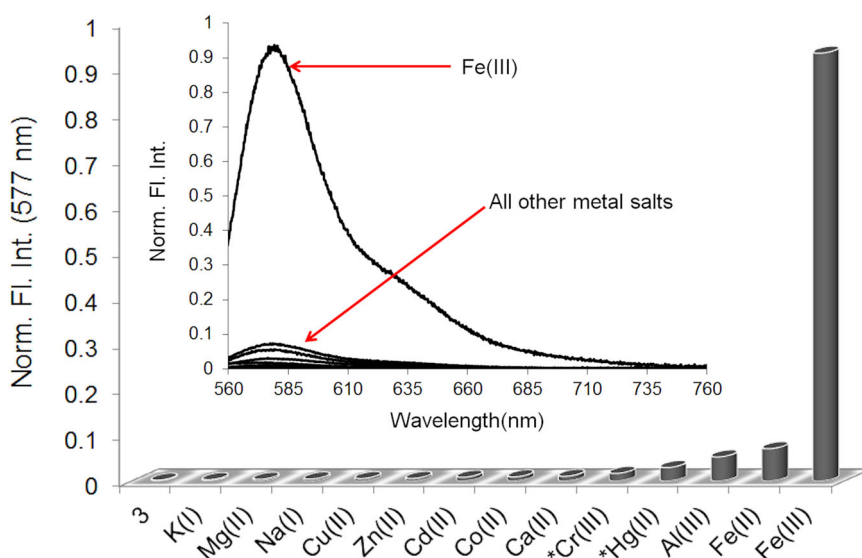


**Figure 9.** Fluorescence screening of metal salts with **3** ( $50\ \mu\text{M}$  in  $\text{CH}_3\text{CN}$  upon addition of three equivalent of metal ions, as their  $\text{ClO}_4^-$  salts (\*Cl $^-$  salt).

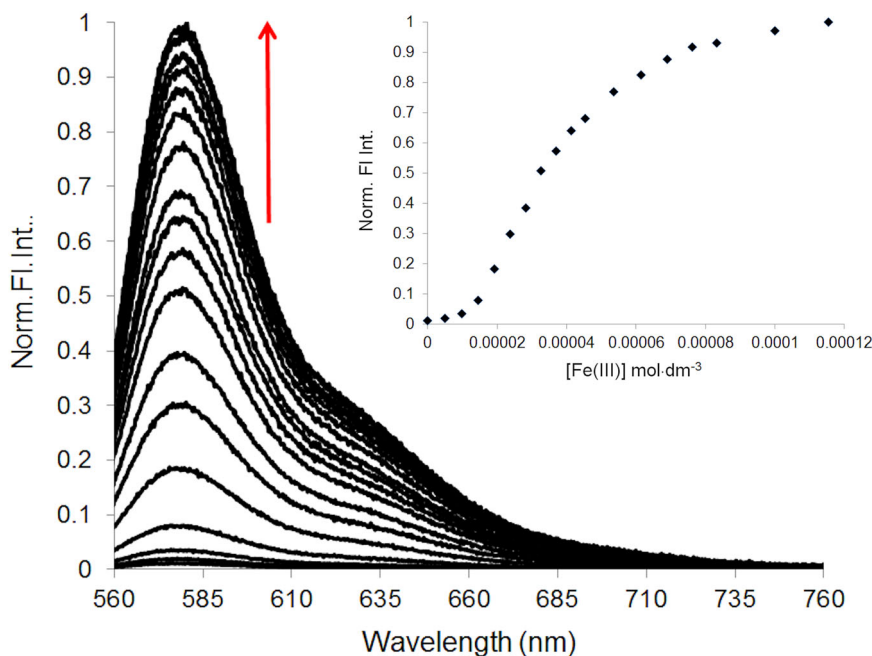


**Figure 10.** Fluorescence titration between **3** upon addition of  $\text{Fe}(\text{ClO}_4)_3$  in a  $5\ \mu\text{mol}\cdot\text{dm}^{-3}$  solution in  $\text{CH}_3\text{CN}:\text{H}_2\text{O}$  (95:5).

more of the ferric salt ( $>5$  equivalents), the excess ferric ion undergoes hydrolysis, which will form hydroxide species that precipitate out of solution or form bridging complexes with the iron metal that has already coordinated to the molecular probe  $[\text{Fe}(\mathbf{3})]^{3+}$ , in agreement with the species required by the non-linear fit model.

### 3.6. Fluorescence spectroscopy

As fluorescence spectroscopy is more sensitive than absorbance, we investigated the fluorometric response of **3** towards the same metal salts ( $\text{Na}^+$ ,  $\text{K}^+$ ,  $\text{Ca}^{2+}$ ,  $\text{Mg}^{2+}$ ,  $\text{Zn}^{2+}$ ,  $\text{Cd}^{2+}$ ,  $\text{Co}^{2+}$ ,  $\text{Fe}^{2+}$ ,  $\text{Cu}^{2+}$ ,  $\text{Hg}^{2+}$ ,  $\text{Cr}^{3+}$ ,  $\text{Al}^{3+}$  and  $\text{Fe}^{3+}$ ). Ferric ions quench the fluorescence intensity of organic fluorophores [105]. To investigate the extent of the quenching in this system, we calculated the quantum yield ( $\phi$ ) for **3** with ferric ions using the comparative method [49]. The quantum yield was calculated to be 0.029 in ethanol using rhodamine 6G as a reference ( $\phi = 0.95$  in EtOH). To confirm that the reduction emission intensity is due to the quenching of the ferric ion, we calculated the quantum yield of rhodamine 6G- $\text{H}^+$ . This study showed that the quantum yield was ten times higher than that of the iron complex ( $\phi = 0.29$ ), in excellent agreement with other rhodamine B sensors for ferric ions (see ESI, Supporting information Figures S31 and S32) [106]. Upon addition of 30 equivalents of  $\text{Fe}^{3+}$  to a  $\text{CH}_3\text{CN}$  of **3** ( $5 \mu\text{mol}\cdot\text{dm}^{-3}$ ) and exciting at 550 nm, a strong fluorescence emission band at 577 nm was observed. There was no evidence of a fluorescence band appearing on the addition of other metal ions (Figure 9), strongly suggesting that **3** is selective for ferric ions. To further investigate the interaction of **3** with  $\text{Fe}^{3+}$ , fluorescence titrations were carried out in  $\text{H}_2\text{O}-\text{CH}_3\text{CN}$  solution. The addition of increasing concentrations of  $\text{Fe}^{3+}$  resulted in a gradual increase of fluorescence intensity at 577 nm (Figure 10). The binding affinity was calculated by the nonlinear regression curve fitting program *HypSpec* using different speciation in the model. The association constant was calculated to be  $\log K_{11} = 4.54$  [50].

Considering there were subtle fluorescence changes for the other metal ions, we carried out competition experiments with metal ions that can exhibit cross-sensitivity and reactivity to eliminate false positives in cell studies. A solution of **3** in  $\text{CH}_3\text{CN}$ -MES buffer (9:1, 1 mM, pH 5.5) ( $5 \mu\text{mol}\cdot\text{dm}^{-3}$ ) contained  $150 \mu\text{mol}\cdot\text{dm}^{-3}$  of metal salts ( $\text{Al}^{3+}$ ,  $\text{Cr}^{3+}$ ,  $\text{Fe}^{2+}$ ,  $\text{Zn}^{2+}$ ,  $\text{Cd}^{2+}$ ,  $\text{Cu}^{2+}$ ,  $\text{Na}^+$ ,  $\text{K}^+$ ,  $\text{Co}^{2+}$  and  $\text{Hg}^{2+}$ ). Once the solution reached equilibrium,  $166 \mu\text{mol}\cdot\text{dm}^{-3}$  ferric perchlorate was added and an increase in fluorescence was observed in all cases (see ESI, Supporting information Figure S36). There was no significant interference with the fluorescence intensity. There was a noticeable decrease with  $\text{Cu}^{2+}$ ,  $\text{Hg}^{2+}$ , and  $\text{Cd}^{2+}$  ions which is not surprising as these metal ions are known to quench fluorescence intensity [107, 108]. This suggests that **3** can be used as a selective fluorescent chemosensor for recognition of  $\text{Fe}^{3+}$  ion in the presence of other metal ions.

An important facet of molecular sensor design is the concept of reversibility. If a molecular probe is to be reused for treatment over several iterations in real applications, it should show reversibility, otherwise, it would be a “one shot” chemodosimeter [109]. To demonstrate the reversibility of **3** with  $\text{Fe}^{3+}$  ions the siderophore DFB (desferoxamine B) was used to scavenge the ferric ion, as it is well known that siderophores target ferric ions with very high binding affinities [68, 69, 110]. A solution of **3** and  $\text{Fe}^{3+}$  ions (five equivalents of  $\text{Fe}^{3+}$  ions to  $20 \mu\text{mol}\cdot\text{dm}^{-3}$  solution) in  $\text{CH}_3\text{CN}$  (see ESI, Supporting information Figure S38) was prepared. Fluorescence was quenched upon addition of DFB as it stripped the  $\text{Fe}^{3+}$  ions from the  $[\text{Fe}(\text{3})]^{3+}$  complex, returning **3** to its original lactam state, but this was reversed upon addition of two equivalents of 2 mM  $\text{Fe}^{3+}$  ions. The observation confirms that **3** is a reversible fluorescent

probe for  $\text{Fe}^{3+}$  ions and the spectral response of **3** to  $\text{Fe}^{3+}$  ions is due to chelation-induced ring-opening of the rhodamine spirolactam. To determine the limit of detection (LoD) the method of least squares was used to give a line of regression. The confidence limit of the slope is defined as  $b \pm t_{sb}$ , where  $t$  is the  $t$ -value taken from the desired confidence and  $n-2$  degrees of freedom. In our experiment, we chose a 95% confidence level ( $t$ -value 2.306,  $df = 10$ ) (see ESI, [Figure S39](#)). It is generally accepted that the LoD is the analyte concentration giving a signal equal to the blank signal plus three standard deviations from the blank, i.e.  $y = y_B \pm 3S_B$ . The calculated LoD value for **3** was  $4 \times 10^{-7} \text{ mol} \cdot \text{dm}^{-3}$  ( $\approx 27 \text{ ppb}$ ).

### 3.7. Confocal microscopy

The solution studies described were carried out in an organic-aqueous mixture (95:5 or 90:10) and this high concentration of organic solvent would certainly be an extreme environment for cells to thrive. For a long time it was believed that any amount of organic solvent was severe for microorganisms [111]. However, Inoue and Horikoshi showed that a strain of *Pseudomonas putida*, a Gram negative bacterium, could actively grow in the presence of 50% toluene solution [105], which was a surprising result at the time. Since this original study, both Gram-negative and Gram-positive bacteria have been found to tolerate high levels of organic solvents [112–114]. This work suggests that bacteria have evolved their biochemical mechanisms to endure these harsh conditions. Even though there is ample evidence that bacteria can tolerate organic solvents, it is generally accepted that any biological studies that are carried out in an organic environment should be kept to a minimum with a 5–15% organic solvent-to-aqueous ratio being acceptable [106]. This ratio is often used to solubilize molecular probes so they can be utilized in the cell medium. Knowing that bacteria can thrive in an organic solvent, a 10% organic solvent system was used to show that ferric ions can be detected in a Gram-positive bacterium.

Chemosensor **3** was also used to detect the free intracellular iron in bacterial cells ([Figure 11](#)). The Gram-positive bacterium *Staphylococcus aureus* was used as it can sequester and use intracellular iron in some of its virulence factor pathways. Bacterial cells were grown for 3 h in TSB, treated with  $\text{FeCl}_3$  ( $100 \mu\text{mol} \cdot \text{dm}^{-3}$ ), and incubated for a further 30 min. The cells were collected by centrifugation, washed twice with sterile double distilled water, and treated with  $100 \mu\text{L}$  of 1 mM of probe **3**. As a control, bacterial cells grown under the same condition as above were also treated with **3** without additional iron. A phase-contrast image of the bacteria was first taken to visualize cells, and the same field was laser scanned in cy3/rhodamine settings with emission and excitation wavelengths of 550 and 580 nm, respectively, to detect fluorescence. Equal numbers of bacteria were observed in both test and control, but red fluorescence was only detected for those treated with iron ([Figure 9](#)). This suggests that the fluorescence produced in the test is due to free intracellular iron detected by the chemosensor and not background fluorescence. The results showed that **3** could be used to detect free intracellular iron in prokaryotic cells like bacteria.

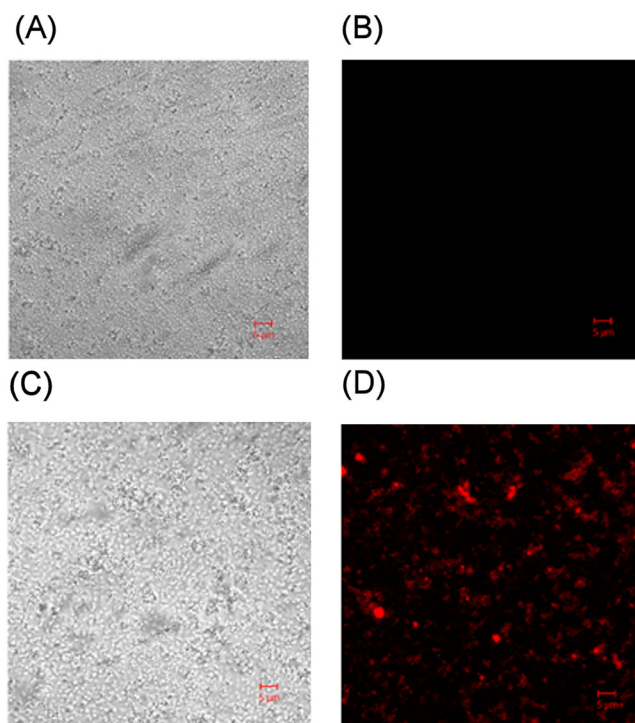


**Figure 11.** Confocal microscopy for detecting intracellular free iron using **3**. Phase-contrast images (A and C) and fluorescence images (B and D) of *S. aureus*. The upper panel is the iron-free control.

#### 4. Conclusion

Many molecular probes that are designed to bind  $\text{Fe}^{3+}$  ions often fail to consider the potential for interference from other trivalent species, in particular,  $\text{Cr}^{3+}$  and  $\text{Al}^{3+}$  ions [78, 81, 115–117]. We believe that this is intentional as these ions are also hard Lewis acids, which can also have high affinities similar to  $\text{Fe}^{3+}$  ions and elicit optical responses. There are a small number of reports of probes that do take  $\text{Al}^{3+}$  into consideration [7, 118] and, ironically, the  $\text{Al}^{3+}$  ion has turned out to be helpful in our studies. We have used 2D NMR to investigate the binding mode of  $\text{Al}^{3+}$  to these probes, as this gave insight into the  $\text{Fe}^{3+}$  coordination environment.

Many ferric ion probes reported in the literature are a little misleading, often claiming that their sensors can monitor ferric ions under conditions in which ferric ions alone cannot exist, a phenomenon we have observed in our own laboratory. This work is the first example of a rhodamine probe utilized to monitor ferric ions in a prokaryotic system, *Staphylococcus aureus*. Whereby, the phase-contrast images, besides showing the presence of bacteria, also showed the presence of fairly equal numbers of cells in both the test and negative control, which suggests that the fluorescence signal is due to the presence of free intracellular iron detected by **3** and not due to any background fluorescence. It is a significant result as this is one of a few examples where iron can be confidently detected in bacteria cells. Rhodamine probes have previously been used to detect intracellular iron in eukaryotic living cells; however, the

published work is questionable as eukaryotic cells have low levels of  $\text{Fe}^{3+}$  ions, required for cell growth, already present. Therefore, often, the "model" systems (i.e. no iron added) already exhibit an emission signal as it is very difficult to grow eukaryotic cells that are iron-free.

In summary, we have synthesized and characterized a new fluorescent "turn-on probe" for  $\text{Fe}^{3+}$  ions, which operates in  $\text{CH}_3\text{CN}$ -MES buffer. The chemosensor exhibits high fluorescence enhancement and selectivity for ferric ions over other metal ions. Binding was also studied by  $^1\text{H}$  NMR, IR-spectroscopy, and DFT calculations. Confocal microscopy experiments showed that **3** can monitor free intracellular iron in the Gram-positive bacterium *Staphylococcus aureus*.

## Funding

KJW would like to thank the NSF (OCE-0963064 and CHE-0840390 for the Acquisition of a cyber accessible 400 MHz NMR at the University of Southern Mississippi) for financial support. PJC thanks the US Army Research Office for funding computational resources (Contract W911NF-15-1-0624). Additional support for the study was made possible by the Mississippi INBRE, an Institutional Development Award (IDeA) from the National Institute of General Medical Sciences (grant number P20GM103476).

## Accession codes

CCDC 1560969 contain the supplementary crystallographic data for this paper. These data can be obtained via XXXX, or by contacting the Cambridge Crystallographic Data Centre, 12 Union Road, Cambridge CB2 1EZ, UK; Fax +44 1223 336033.

## ORCID

Peter J. Cragg  <http://orcid.org/0000-0002-6134-2093>

Karl J. Wallace  <http://orcid.org/0000-0003-4541-7523>

## References

- [1] J. Yin, Y. Hu, J. Yoon. *Chem. Soc. Rev.*, **44**, 4619 (2015).
- [2] Y.L. Pak, K.M.K. Swamy, J. Yoon. *Sensors (Basel)*, **15**, 24374 (2015).
- [3] K.P. Carter, A.M. Young, A.E. Palmer. *Chem. Rev.*, **114**, 4564 (2014).
- [4] C.D. Fryar, Q. Gu, C.L. Ogden. Anthropometric reference data for children and adults: United States, 2007-2010. U.S. Department of health and human services, *Centers for Disease Control and Prevention*, Washington DC, Vol. 252 (2012).
- [5] Y. Yu, D.S. Kalinowski, Z. Kovacevic, A.R. Siafakas, P.J. Jansson, C. Stefani, D.B. Lovejoy, P.C. Sharpe, P.V. Bernhardt, D.R. Richardson. *J. Med. Chem.*, **52**, 5271 (2009).
- [6] S. Epsztejn, H. Glickstein, V. Picard, I.N. Slotki, W. Breuer, C. Beaumont, V.L. Cabantchik. *Blood*, **94**, 3593 (1999).
- [7] S.K. Sahoo, D. Sharma, R.K. Bera, G. Crisponi, J.F. Callan. *Chem. Soc. Rev.*, **41**, 7195 (2012).
- [8] P. Aisen, M. Wessling-Resnick, E.A. Leibold. *Curr. Opin. Chem. Biol.*, **3**, 200 (1999).
- [9] A. Jacobs. *Blood*, **50**, 433 (1977).
- [10] O. Kakhlon, Z.I. Cabantchik. *Free Radic. Biol. Med.*, **33**, 1037 (2002).
- [11] M. Kruszewski. *Mutat. Res.*, **531**, 81 (2003).
- [12] M. Valko, C.J. Rhodes, J. Moncol, M. Izakovic, M. Mazur. *Chem. Biol. Interact.*, **160**, 1 (2006).

- [13] B. Halliwell, J.M.C. Gutteridge. *Methods Enzymol.*, **186**, 1 (1990).
- [14] S. Rivera-Mancia, I. Pérez-Neri, C. Ríos, L. Tristán-López, L. Rivera-Espinosa, S. Montes. *Chem. Biol. Interact.*, **186**, 184 (2010).
- [15] K.J. Thompson, S. Shoham, J.R. Connor. *Brain Res. Bull.*, **55**, 155 (2001).
- [16] H. Kozłowski, A. Janicka-Kłos, J. Brasun, E. Gaggelli, D. Valensin, G. Valensin. *Coord. Chem. Rev.*, **253**, 2665 (2009).
- [17] P. Zatta, D. Drago, S. Bolognin, S.L. Sensi. *Trends Pharmacol. Sci.*, **30**, 346 (2009).
- [18] J.D. Haas, T.I.V. Brownlie. *J. Nutr.*, **131**, 676S (2001).
- [19] C. Brugnara. *Clin. Chem.*, **49**, 1573 (2003).
- [20] M. Kumar, R. Kumar, V. Bhalla, P.R. Sharma, T. Kaur, Y. Qurishi. *Dalton Trans.*, **41**, 408 (2012).
- [21] M. Kumar, R. Kumar, V. Bhalla. *Tetrahedron Lett.*, **51**, 5559 (2010).
- [22] V. Bhalla, N. Sharma, N. Kumar, M. Kumar. *Sens. Actuators B*, **178**, 228 (2013).
- [23] V. Bhalla, A. Gupta, M. Kumar. *Dalton Trans.*, **42**, 4464 (2013).
- [24] M.H. Lee, T. van Giap, S.H. Kim, Y.H. Lee, C. Kang, J.S. Kim. *Chem. Commun. (Camb)*, **46**, 1407 (2010).
- [25] M.H. Lee, H. Lee, M.J. Chang, H.S. Kim, C. Kang, J.S. Kim. *Dyes Pigm.*, **130**, 245 (2016).
- [26] D.R. Richardson, P.C. Sharpe, D.B. Lovejoy, D. Senaratne, D.S. Kalinowski, M. Islam, P.V. Bernhardt. *J. Med. Chem.*, **49**, 6510 (2006).
- [27] N.C. Lim, S.C. Pavlova, C. Brückner. *Inorg. Chem.*, **48**, 1173 (2009).
- [28] S.M. Cohen, M. Meyer, K.N. Raymond. *J. Am. Chem. Soc.*, **120**, 6277 (1998).
- [29] R.J. Ward, F.A. Zucca, J.H. Duyn, R.R. Crichton, L. Zecca. *Lancet. Neurol.*, **13**, 1045 (2014).
- [30] R.J. Ward, D.T. Dexter, R.R. Crichton. *J. Trace Elem. Med. Biol.*, **31**, 267 (2015).
- [31] R. Cusnir, C. Imberti, R.C. Hider, P.J. Blower, M.T. Ma. *Int. J. Mol. Sci.*, **18**, 1 (2017).
- [32] A.J.M. Messenger, R. Barclay. *Biochem. Educ.*, **11**, 54 (1983).
- [33] T.C. Johnstone, E.M. Nolan. *Dalton Trans.*, **44**, 6320 (2015).
- [34] D. Perkins-Balding, M. Ratliff-Griffin, I. Stojiljkovic. *Microbiol. Mol. Biol. Rev.*, **68**, 154 (2004).
- [35] A. Pandey, F. Bringel, J.-M. Meyer. *Appl. Microbiol. Biotechnol.*, **40**, 765 (1994).
- [36] M. Imbert, R. Blondeau. *Curr. Microbiol.*, **37**, 64 (1998).
- [37] K.H. Ebrahimi, E. Bill, P.-L. Hagedoorn, W.R. Hagen. *Nat. Chem. Biol.*, **8**, 941 (2012).
- [38] I.U. Heinemann, M. Jahn, D. Jahn. *Arch. Biochem. Biophys.*, **474**, 238 (2008).
- [39] A.S. Fleischhacker, P.J. Kiley. *Curr. Opin. Chem. Biol.*, **15**, 335 (2011).
- [40] E. Banin, M.L. Vasil, E.P. Greenberg. *Proc. Natl. Acad. Sci. USA*, **102**, 11076 (2005).
- [41] J. Kluytmans, A. van Belkum, H. Verbrugh. *Clin. Microbiol. Rev.*, **10**, 505 (1997).
- [42] N.R. Chereddy, S. Thennarasu, A.B. Mandal. *Dalton Trans.*, **41**, 11753 (2012).
- [43] S.-R. Liu, S.-P. Wu. *Sens. Actuators B*, **171–172**, 1110 (2012).
- [44] M. Tian, X. Peng, J. Fan, J. Wang, S. Sun. *Dyes Pigm.*, **95**, 112 (2012).
- [45] J. Wang, Y. Li, N.G. Patel, G. Zhang, D. Zhou, Y. Pang. *Chem. Commun. (Camb)*, **50**, 12258 (2014).
- [46] S. Goswami, K. Aich, S. Das, A.K. Das, D. Sarkar, S. Panja, T.K. Mondal, S. Mukhopadhyay. *Chem. Commun. (Camb)*, **49**, 10739 (2013).
- [47] S.B. Maity, P.K. Bharadwaj. *Inorg. Chem.*, **52**, 1161 (2013).
- [48] Y.-S. Wu, C.-Y. Li, Y.-F. Li, J.-L. Tang, D. Liu. *Sens. Actuators B*, **203**, 712 (2014).
- [49] A.T.R. Williams, S.A. Winfield, J.N. Miller. *Analyst*, **108**, 1067 (1983).
- [50] P.; Gans. Protonic Software: Leeds, UK (2014)
- [51] Nonius; Nonius BV, Delft, The Netherlands (2000)
- [52] Z. Otwinowski, W. Minor. In *Methods in Enzymology*, C.W. Carter Jr., R.M. Sweet (Eds.), Vol. 276, Academic Press, New York (1997).
- [53] A. Altomare, M.C. Burla, M. Camalli, G.L. Casciaro, C. Giacovazzo, A. Guagliardi, A.G.G. Moliterni, G. Polidori, R. Spagna. *J. Appl. Crystallogr.*, **32**, 115 (1999).
- [54] G.M. Sheldrick. *Acta Crystallogr. C Struct. Chem.*, **71**, 3 (2015).
- [55] P. Gans. Protonic Software: Leeds, UK (2016)
- [56] Z. Jin, D.-X. Xie, Z.-B. Zhang, Y.-J. Gong, W. Tan. *Anal. Chem.*, **84**, 4253 (2012).



- [57] D.J. Hutchinson, L.R. Hanton, S.C. Moratti. *Inorg. Chem.*, **49**, 5923 (2010).
- [58] V. Dujols, F. Ford, A.W. Czarnik. *J. Am. Chem. Soc.*, **119**, 7386 (1997).
- [59] M. Beija, C.A.M. Afonso, J.M.G. Martinho. *Chem. Soc. Rev.*, **38**, 2410 (2009).
- [60] H.N. Kim, M.H. Lee, H.J. Kim, J.S. Kim, J. Yoon. *Chem. Soc. Rev.*, **37**, 1465 (2008).
- [61] X. Chen, T. Pradhan, F. Wang, J.S. Kim, J. Yoon. *Chem. Rev.*, **112**, 1910 (2012).
- [62] Y. Ma, W. Luo, P.J. Quinn, Z. Liu, R.C. Hider. *J. Med. Chem.*, **47**, 6349 (2004).
- [63] M. Kumar, R. Kumar, V. Bhalla. *Org. Lett.*, **13**, 366 (2011).
- [64] A.B. Davis, F.R. Fronczek, K.J. Wallace. *Acta Crystallogr.*, **E72**, 1032 (2016).
- [65] A.M. Mallet, A.B. Davis, D.R. Davis, J. Panella, K.J. Wallace, M. Bonizzoni. *Chem. Commun. (Camb)*, **51**, 16948 (2015).
- [66] E. Manandhar, P.J. Cragg, K.J. Wallace. *Supramol. Chem.*, **26**, 141 (2014).
- [67] E. Manandhar, J.H. Broome, J. Myrick, W. Lagrone, P.J. Cragg, K.J. Wallace. *Chem. Commun. (Camb)*, **47**, 8796 (2011).
- [68] K.M. Orcutt, W.S. Jones, A. McDonald, D. Schrock, K.J. Wallace. *Sensors (Basel)*, **10**, 1326 (2010).
- [69] K.J. Wallace, M. Gray, Z. Zhong, V.M. Lynch, E.V. Anslyn. *Dalton Trans.*, 2436 (2005).
- [70] A.B. Davis, R.E. Lambert, F.R. Fronczek, P.J. Cragg, K.J. Wallace. *New J. Chem.*, **38**, 4678 (2014).
- [71] I. Walton, M. Davis, L. Yang, Y. Zhang, D. Tillman, W.L. Jarrett, M.T. Huggins, K.J. Wallace. *Magn. Reson. Chem.*, **49**, 205 (2011).
- [72] W. Walton, D. Marauo, L. Munro, V.J. Catalano, P.J. Cragg, M.T. Huggins, K.J. Wallace. *Org. Lett.*, **14**, 2686 (2012).
- [73] K. Kellett, J.H. Broome, M. Zloh, S.B. Kirton, S. Fergus, U. Gerhard, J.L. Stair, K.J. Wallace. *Chem. Commun. (Camb)*, **52**, 7474 (2016).
- [74] J.-E. Backvall. *Modern Oxidation Methods*, Wiley-VCH, Weinham (2003).
- [75] G. Tojo, M. Fernandez. *Oxidation of Alcohols to Aldehydes and Ketones: A Guide to Current Common Practice*, Springer Science & Business Media, New York (2006). <https://www.springer.com/gp/book/9780387236070>
- [76] Q.A. Best, R. Xu, M.E. McCarroll, L. Wang, D.J. Dyer. *Org. Lett.*, **12**, 3219 (2010).
- [77] S. Kenmoku, Y. Urano, H. Kojima, T. Nagano. *J. Am. Chem. Soc.*, **129**, 7313 (2007).
- [78] W. Huang, C. Song, C. He, G. Lv, X. Hu, X. Zhu, C. Duan. *Inorg. Chem.*, **48**, 5061 (2009).
- [79] J.D. Chartres, M. Busby, M.J. Riley, J.J. Davis, P.V. Bernhardt. *Inorg. Chem.*, **50**, 9178 (2011).
- [80] Z. Yang, M. She, B. Yin, J. Cui, Y. Zhang, W. Sun, J. Li, Z. Shi. *J. Org. Chem.*, **77**, 1143 (2012).
- [81] X. Chen, X. Meng, S. Wang, Y. Cai, Y. Wu, Y. Feng, M. Zhu, Q. Guo. *Dalton Trans.*, **42**, 14819 (2013).
- [82] A. Sahana, A. Banerjee, S. Lohar, A. Banik, S.K. Mukhopadhyay, D.A. Safin, M.G. Babashkina, M. Bolte, Y. Garcia, D. Das. *Dalton Trans.*, **42**, 13311 (2013).
- [83] Y.J. Kim, C.R. Park. *Inorg. Chem.*, **41**, 6211 (2002).
- [84] M.R. Rosenthal. *J. Chem. Educ.*, **50**, 331 (1973).
- [85] G. Herzberg. *Infrared and Raman Spectra*, Litton Educational Publishing, New York (1944).
- [86] A.S. Goldin, R.J. Velten, G.W. Frishkorn. *Anal. Chem.*, **31**, 1490 (1959).
- [87] R.D. Armstrong, D.F. Porter, H.R. Thirsk. *J. Phys. Chem.*, **72**, 2300 (1968).
- [88] A.D.G. Johnson. Dissertation, The University of Southern Mississippi (2020).
- [89] P. Gans. Protonic Software: Leeds, UK (2009).
- [90] K.N. Raymond, C.J. Carrano. *Acc. Chem. Res.*, **12**, 183 (1979).
- [91] E. Griffiths. *Iron and Infection*, In Iron and infection, Vol. **69**, 2nd Edn, pp. 69–137, Chichester UK (1987). [https://books.google.com/books/about/Iron\\_and\\_Infection.html?id=BwSrAAAAMAAJ&source=kp\\_book\\_description](https://books.google.com/books/about/Iron_and_Infection.html?id=BwSrAAAAMAAJ&source=kp_book_description)
- [92] K.G. Wooldridge, P.H. Williams. *FEMS Microbiol. Rev.*, **12**, 325 (1993).
- [93] R.C. Hider, X. Kong. *Nat. Prod. Rep.*, **27**, 637 (2010).
- [94] K.J. Wallace, A.D.G. Johnson, W.S. Jones, E. Manandhar. *Supramol. Chem.*, **30**, 353 (2018).



- [95] A.N. Pham, A.L. Rose, A.J. Feitz, T.D. Waite. *Geochim. Cosmochim. Acta*, **70**, 640 (2006).
- [96] M. Zhu, C. Frandsen, A.F. Wallace, B. Legg, S. Khalid, H. Zhang, S. Morup, J.F. Banfield, G.A. Waychunas. *Geochim. Cosmochim. Acta*, **172**, 247 (2016).
- [97] P.G. Daniele, C. Rigano, S. Sammartano, V. Zelano. *Talanta*, **41**, 1577 (1994).
- [98] P. Hemmes, L.D. Rich, D.L. Cole, E.M. Eyring. *J. Phys. Chem.*, **75**, 929 (1971).
- [99] R.L. Martin, J.P. Hay, L.R. Pratt. *J. Phys. Chem. A*, **102**, 3565 (1998).
- [100] D.G. Kinniburgh, D.M. Cooper. *Environ. Sci. Technol.*, **38**, 3641 (2004).
- [101] A.F. Cotton, G. Wilkinson. *Advanced Inorganic Chemistry: A Comprehensive Text*, John Wiley and Sons, United States (1962).
- [102] P.C. Junk, B.J. McCool, B. Moubaraki, K.S. Murray, L. Spiccia, J.D. Cashion, J.W. Steed. *J. Chem. Soc. Dalton Trans.*, 1024 (2002).
- [103] M. Zhu, B.W. Puls, C. Frandsen, J.D. Kubicki, H. Zhang, G.A. Waychunas. *Inorg. Chem.*, **52**, 6788 (2013).
- [104] R.H. Byrne, W. Yao, Y.-R. Luo, B. Wang. *Marine Chem.*, **97**, 34 (2005).
- [105] J.R. Lakowicz. *Principles of Fluorescence Spectroscopy*, 3rd edn, Springer, New York (2006).
- [106] A.J. Weerasinghe, C. Schmiesing, S. Varaganti, G. Ramakrishna, E. Sinn. *J. Phys. Chem. B*, **114**, 9413 (2010).
- [107] V. Bhalla, M. Kumar, P.R. Sharma, T. Kaur. *Inorg. Chem*, **51**, 2150 (2012).
- [108] J. Wang, L. Long, D. Xie, X. Song. *Sens. Actuators B*, **177**, 27 (2013).
- [109] B. Wang, E.V. Anslyn. *Chemosensors: Principles, Strategies, and Applications*, John Wiley & Sons, Hoboken, New Jersey (2011).
- [110] S.C. Andrews, A.K. Robinson, F. Rodríguez-Quiñones. *FEMS Microbiol. Rev.*, **27**, 215 (2003).
- [111] R. Aono, K. Aibe, A. Inoue, K. Horikoshi. *Agric. Biol. Chem.*, **55**, 1935 (1991).
- [112] D. K. Hong, S.-H. Jang, C. Lee. *J. Mol. Catal. B Enzym.*, 133, S337 (2017).
- [113] Y.N. Sardessai, S. Bhosle. *Biotechnol. Prog.*, **20**, 655 (2004).
- [114] N. Doukyu, H. Ogino. *Biochem. Eng. J.*, **48**, 270 (2010).
- [115] F. Ge, H. Ye, H. Zhang, B.-X. Zhao. *Dyes Pigm.*, **99**, 661 (2013).
- [116] M. Chai, D. Zhang, M. Wang, H. Hong, Y. Ye, Y. Zhao. *Sens. Actuators B*, **174**, 231 (2012).
- [117] Z.-Q. Hu, Y.-C. Feng, H.-Q. Huang, L. Ding, X.-M. Wang, C.-S. Lin, M. Li, C.-P. Ma. *Sens. Actuators B*, **156**, 428 (2011).
- [118] Y. Zhou, H. Zhou, J. Zhang, L. Zhang, J. Niu. *Spectrochim. Acta A Mol. Biomol. Spectrosc.*, **98**, 14 (2012).